

The B3–VLA CSS sample

II. VLBA images at 18 cm

D. Dallacasa^{1,2}, S. Tinti^{1,2,*}, C. Fanti^{3,2}, R. Fanti^{3,2}, L. Gregorini^{3,2}, C. Stanghellini⁴, and M. Vigotti²

¹ Dipartimento di Astronomia, Università di Bologna, Via Ranzani 1, 40127 Bologna, Italy

² Istituto di Radioastronomia del CNR, via Gobetti 101, 40129 Bologna, Italy

³ Dipartimento di Fisica, Università di Bologna, via Irnerio 46, 40126 Bologna, Italy

⁴ Istituto di Radioastronomia del CNR, CP 141, 96017 Noto SR, Italy

Received 22 January 2002 / Accepted 11 April 2002

Abstract. VLBA observations at 18 cm are presented for 28 Compact Steep-spectrum radio Sources (CSSs) from the B3–VLA CSS sample. These sources were unresolved in previous VLA observations at high frequencies or their brightness distribution was dominated by an unresolved steep spectrum component. More than half of them also showed a low frequency turnover in their radio spectrum. The VLBA images display in most cases a compact symmetric structure. Only in a minority of cases complex morphologies are present.

Key words. galaxies: active – radio continuum: galaxies – quasars: general

1. Introduction

The population of CSSs (Compact Steep-spectrum Sources) & GPSs (GHz Peaked-spectrum Sources) (see O’Dea, 1998 for a review) has received recently an increasing attention as at least the two sided (or symmetric) objects of this class are considered to be the young stage in the radio source evolution (Fanti et al. 1995; Readhead et al. 1996), from the Compact (CSO, size $< 1 h^{-1}$ kpc)¹ through the Medium (MSO, $1 h^{-1}$ kpc $<$ size $< 20 h^{-1}$ kpc) to the Large Symmetric Object (LSO, size $> 20 h^{-1}$ kpc). A strong support for this interpretation comes from the large expansion velocities recently measured in a handful of sub-kpc sources (see compilation in Fanti 2000 and references therein) and from the determination of the radiative ages of a larger number of CSSs spanning a range of linear size from sub-kpc to $\sim 20 h^{-1}$ kpc (Murgia et al. 1999).

Starting from the seminal paper by Baldwin 1982, models for radio source evolution have been presented by several authors which link the CSS/GPS population to the larger size sources, (see e.g. Begelman 1996; Kaiser & Alexander 1997).

All models essentially predict a decrease of the source luminosity with time, and therefore with increasing source linear size. A key test for the models is the ability to reproduce the distribution of sources in the “Radio Power – Linear Size” ($P_R - LS$) plane (Baldwin 1982). CSSs/GPSs seem to be in the right proportion as compared with model expectations (Fanti et al. 1995; Readhead et al. 1996). However, from the samples studied so far the statistics have been not very large and suspicions were raised on some “irregularities” in the LS distribution (O’Dea & Baum 1997) and on the, perhaps too high, number of very small size CSSs, the GPSs (Polatidis et al. 1999; Fanti & Fanti 2001).

Recently we have selected a new sample of CSSs from the B3–VLA catalogue (Vigotti et al. 1989) aimed at increasing significantly the statistics on sources with LS in the range $0.4 h^{-1} \leq LS(\text{kpc}) \leq 20 h^{-1}$ (Fanti et al. 2001, hereafter referred to as Paper I). This sample, consisting of 87 CSSs ($LS \leq 20 h^{-1}$ kpc), has VLA observations at 1.4 GHz (A and C configurations), 5 and 8.4 GHz (both A configuration). About 50% of these sources were not resolved or were poorly resolved even at 8.4 GHz (beam size $\sim 0.2''$). For them two VLBI observing projects were undertaken with the VLBA and EVN & MERLIN.

This paper reports on the results of the VLBA observations of the most compact sources. The EVN & MERLIN observations instead are presented in a companion paper by Dallacasa et al. (2002, Paper III).

Send offprint requests to: D. Dallacasa,
e-mail: ddallaca@ira.cnr.it

* Present address: S. Tinti, SISSA, via Beirut 2–4,
34014 Trieste, Italy.

¹ $H_0 = 100 h \text{ km s}^{-1} \text{ Mpc}^{-1}$, $q_0 = 0.5$.

Table 1. The VLBA sample: see text for a description of the columns.

Source	Id	m_R	z	LAS mas	$\log P_{0.4\text{GHz}}$ W/Hz h^{-2}	$S_{1.67}^{\text{VLA}}$ mJy	$S_{1.67}^{\text{VLBA}}$ mJy	LAS_{VLBA} mas	LLS kpc h^{-1}	Morph.
(1)	(2)	(3)	(4)	(5)	(6)	(7)	(8)	(9)	(10)	(11)
0039+373	G		1.006	100	27.37	784	779	120	0.50	CSO
0147+400	E			100	>26.6	631	563	95	~0.40	scJ? [‡]
0703+468	E			80	>26.6	1392	1356	75	~0.32	CSO
0800+472	* E			1000	>26.8	769	447	160	~0.67	scJ? [‡]
0809+404	* G		0.551	1200	26.90	929	522	80	0.28	?
0822+394	G		1.180	50	27.33	1003	942	70	0.30	CSO
0840+424A	E			80	>26.8	1243	1187	135	~0.57	CSO
1007+422	* E			130	>26.4	370	313	265	~1.12	MSO
1008+423	E			50	>26.5	521	498	115	~0.48	CSO
1016+443	G	19.7	0.33	R 110	26.11	287	266	155	0.44	CSO
1044+454	* G	24.8	4.10	K 1000	28.82	352	311	175	0.55	?
1049+384	* G	20.9	1.018	100	27.14	574	502	210	0.89	CSO?
1133+432	E			70	>26.3	1247	1265	45	~0.20	CSO
1136+383	* E			50	>26.4	400	377	70	~0.28	CSO
1136+420	G	21.7	0.829	1000	^a 26.9	402	279	120	0.49	?
1159+395	G	23.4	2.370	50	27.57	535	498	70	0.26	CSO
1225+442	G	18.2	0.22	R 200	27.50	316	291	420	0.95	CSO
1242+410	Q	19.7	0.811	40	27.08	1215	1126	70	0.29	CSO?
1314+453A*	G	21.8	1.544	160	27.77	574	493	185	0.79	CSO
1340+439	E			70	>26.5	447	397	130	~0.56	CSO
1343+386	* Q	17.5	1.844	110	27.70	793	717	130	0.54	CSO
1432+428B*	E			40	>26.3	809	706	50	~0.21	CSO
1441+409	E			100	>26.7	834	768	130	~0.56	CSO
1449+421	E			80	>26.9	639	592	120	~0.50	CSO
2304+377	G	19.7	0.40	R 100	26.44	1299	1217	150	0.49	CSO
2330+402	E			70	>26.7	730	705	100	~0.43	CSO
2348+450	* G		0.978	200	27.36	630	520	310	1.32	MSO
2358+406	E			80	>26.8	1159	1161	120	~0.47	CSO

^a The value given in Fanti et al. (2001) is wrong.

[‡] Steep-core Jet: elongated structure, very asymmetric in brightness, where the brightest component is at one source extremity and has a steep spectrum.

2. The source list and VLBA observations

Among the twenty-eight sources selected for VLBA observations, twenty-four are unresolved or slightly resolved (angular size $\leq 0.2''$) in the VLA 8.4 GHz observations. The remaining four sources are dominated in flux density by an unresolved or slightly resolved component, with the additional presence of some weaker emission (bringing the overall size up to $\sim 1''$, Table 1) whose connection with the compact feature is unclear. In addition about half of the sample sources present a low frequency turnover in the total spectrum which is usually considered an indication of compactness in some sub-component. All these sources, therefore, deserved further investigation.

The selected sample is presented in Table 1. The content of the table is the following.

Column 1: Source name; an “*” refers to a note (Sect. 4);

Column 2: Optical Identification (Id) from Paper I (G = galaxy, Q = quasar, E = no known optical counterpart);

Column 3: R magnitude;

Column 4: redshift; “K” and “R” indicate that the redshift is estimated by photometric measurements in the respective optical band (see Paper I for details);

Column 5: VLA Largest Angular Size (LAS) in mas, from Paper I;

Column 6: $\log P_{0.4\text{GHz}}$ (P in W/Hz h^{-2}); for E sources lower limits to the radio power have been computed assuming $z = 0.5$ (see also Paper I for a wider discussion);

Column 7: flux density (mJy), interpolated at 1.67 GHz from the 1.4 GHz NVSS (Condon et al. 1998) and the 5 GHz VLA data from Paper I;

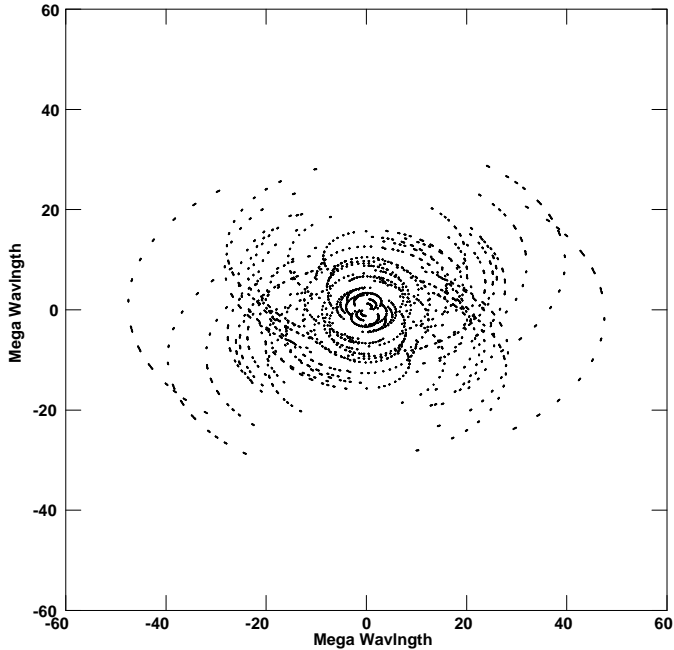


Fig. 1. Typical uv coverage.

Column 8: VLBA 1.67 GHz flux density (mJy), measured on the images presented here (see Sect. 3);

Column 9: VLBA Largest Angular Size (mas);

Column 10: Largest Linear Size (LLS , kpc h^{-1}) from VLBA data; for E sources $z = 1.05$ was assumed (see Paper I for details) and LLS , given with a leading “ \sim ”, must be considered a lower limit;

Column 11: overall morphology (see Sect. 5).

The VLBA observations were carried out in February 2000 at the frequency of 1.67 GHz, with a recording band-width of 32 MHz at 64 Mbps. Each source was observed for a total of about 1 hour, spread into 10 to 15 short scans in order to improve the uv coverage. A typical example of uv coverage is given in Fig. 1. As no single VLA antenna was available, the shortest baseline is Pie Town–Los Alamos (~ 1.3 M λ). This may have caused some flux density losses in the more extended sources/components.

3. Data reduction

The data were correlated with the NRAO processor at Socorro. Amplitude calibration was obtained using the system temperature measured at the various antennas during the observations and the gain information provided by NRAO. Consistency checks were performed with OQ208 and DA193, whose amplitudes were found to be generally within 2% of what expected.

Standard editing and fringe-fitting were applied. Most sources provided fringes with high signal-to-noise ratio on all baselines.

Radio images were obtained using AIPS, after a number of phase self-calibrations, ended by a final amplitude self-calibration. The last step was made with great care, as the gain self-calibration tends to depress the total flux

density when extended components are poorly sampled in uv coverage. Generally the gain corrections from self-calibration were $<3\%$. In those sources in which they were $\geq 3\%$, or in which the total flux density decreased by more than 1–2%, they were not considered.

The rms noise level (1σ), measured on the images far from the sources, is in the range of 0.1–0.2 mJy/beam, comparable to the expected thermal noise. The dynamic range, defined as the ratio of peak brightness to 1σ , is ~ 700 on average, ranging from 300 to a few thousands. The typical resolution is $\sim 4 \times 8$ mas. We must remark that the LLS determined on the VLBA images (Table 1, Col. 9) does not take into account the eventual presence of components completely resolved out by the VLBA observations. We note also that it may exceed the VLA rough estimate due to the source structure (e.g. a double edge-brightened source will appear smaller when fitted by a single Gaussian with a resolution smaller than the separation between components).

The total flux density “seen” by VLBA (Table 1, Col. 8) has been measured by integration over the source images using the AIPS task TVSTAT. The brightest sub-structures of each source were fitted by a Gaussian model (task JMFIT) which allows to obtain total flux density, the beam-deconvolved Half Maximum Widths (HMW) and major axis position angle (PA). Sub-components are referred to as North (N), South (S), East (E), West (W) and Central (Ce). When a component is split into more pieces, a digit (1, 2, etc.) is added (e.g. N1, N2). Other symbols used are self-explanatory. The source images are shown in Fig. 3. The labels are marked on the images, next to each sub-component. The parameters of the brightest sub-components are given in Table 2, which has the following layout:

Columns 1, 2: Source name and sub-component label; an “*” indicates that the component is extended and its flux density is obtained by TVSTAT (see text);

Column 3: VLBA flux density;

Column 4: deconvolved angular sizes of major and minor axis of a Gaussian component and position angle of the major axis as estimated using the AIPS Gaussian-fitting task JMFIT.

For more extended features, marked by an “*” in Table 2, flux densities are evaluated by means of TVSTAT. For extended structures underlying more compact ones, the flux density is obtained as difference between the integrated flux density and the sum of the sub-component Gaussian fit flux densities.

We have checked the integrated flux densities in our images with the low resolution flux densities obtained by interpolating to our observing frequency the values from the NVSS (Condon et al. 1998) and from the VLA data at 5 GHz from Paper I. The comparison is displayed in Fig. 2.

There is clearly a systematic flux density difference, typically $\gtrsim 5\%$, which could be partially ascribed to calibration uncertainties. For the more extended objects there

Table 2. Observational parameters of source components.

Source		S	θ_1	θ_2	(PA)	Source		S	θ_1	θ_2	(PA)	
(1)	(2)	(mJy)	mas	mas	deg	(1)	(2)	(mJy)	mas	mas	deg	
		(3)	–	(4)	–			(3)	–	(4)	–	
0039+373	N1	229	4.7	4.3	101	1225+442	E1	138	26.6	15.1	88	
	N2	143	11.0	6.8	17		E*	28				
	N*	17					W1	94	46.6	23.3	71	
	S1	303	13.2	6.9	24		W2	35	32.4	10.6	134	
	S*	88					1242+410	S	818	20.8	5.1	26
0147+400	E	208	2.7	2.4	41	N		208	7.7	4.8	53	
	W1	134	11.6	7.6	40	T*		101				
	W2	109	13.7	10.6	26	1314+453		W1	175	26.7	15.6	71
	T*	113						W2	77	31.6	26.9	73
	0703+468	W1	794	7.1	4.01		51	Ce	60	19.0	15.0	143
W*		22					E1	101	28.0	14.6	63	
E1		497	5.7	4.0	80		E2	76	41.4	10.2	65	
E*		44				NW	18	25.0	8.9	82		
0800+472		S1	177	25.5	9.4	49	1340+439	N1	208	9.0	5.2	9
	S2	95	32.4	6.9	70	N2		104	13.9	5.8	44	
	N1	120	36.5	19.2	34	Ce1		38	10.3	1.5	26	
	N2	68	25.6	22.9	60	Ce2		13	7.2	2.2	4	
	N3	24	18.8	11.3	178	S		27	12.0	6.6	83	
0809+404	N	250	16.1	12.2	161	1343+386	S1	541	6.2	5.9	131	
	S	221	17.5	12.2	161		S*	68				
	T*	51					Ce	20	12.8	4.5	170	
	0822+394	E1	424	5.3	3.5		37	N	66	3.5	0.6	171
		E2	269	16.4	3.3		57	N*	20			
W1		153	6.7	4.5	66	1432+428	E1	570	4.9	3.0	106	
W2		97	6.4	3.7	81		E*	25				
0840+424		N1	823	8.2	4.8		10	W	104	11.4	7.5	133
	N2	145	12.5	4.5	169		1441+409	W1	312	6.7	4.2	50
	S1	71	7.1	5.7	50			W2	132	17.1	8.0	43
	S2	137	16.8	11.6	139	Ce1		140	7.6	3.0	63	
	1007+422	S1	238	32.9	15.8	84		Ce2	42	< 3.5	< 3.5	-180
S2		52	22.4	8.7	40	E1		70	8.0	3.1	176	
N		32	40.0	23.5	153	E2	68	17.2	7.3	30		
1008+423		W1	139	12.3	4.4	128	1449+421	N1	121	12.04	7.0	96
		W2	250	12.0	5.3	35		N2	149	5.2	2.7	26
	W*	14				N3		87	8.09	4.1	4	
	Ce	14	12.2	5.2	54	Ce1		15	8.5	2.6	24	
	E	104	27.8	19.4	46	Ce2		58	5.8	3.4	31	
1016+443	N1	109	8.1	5.5	156	2304+377	Ce3	44	8.9	2.1	27	
	N2	67	15.1	3.5	175		S	120	11.0	8.2	60	
	N3	6	15.9	1.6	166		W1	244	4.8	0.2	89	
	S1	27	15.1	7.7	155		W2	671	21.0	6.6	117	
	S2	58	18.9	7.2	5		W3	91	7.1	2.3	104	
1044+454	E1	124	8.3	3.8	106	2330+402	E1	219	4.0	3.3	114	
	E2	138	19.9	17.1	110		E2	41	9.0	5.6	67	
	E*	18					E3	124	28.0	17.8	110	
	W1	24	7.3	4.4	6		W1	332	2.4	1.8	33	
	W2	7	10.6	1.7	177		W*	37				
1049+384	W1	244	7.0	4.1	8	2348+450	E1	62	7.0	4.8	152	
	W2	206	8.7	2.5	119		E2	204	17.5	12.9	164	
	E1	21	< 5.5	< 5.5	-179		E*	70				
	E2	26	5.4	3.6	133		S1	203	5.1	4.1	159	
	1133+432	N	799	3.5	2.9		48	S*	168			
S		460	4.1	3.6	167	N1	75	19.9	14.4	93		
1136+383		N1	134	5.2	3.0	170	N*	74				
		N2	93	10.1	4.1	10	2358+406	S1	681	5.6	3.9	143
		Ce	23	8.2	3.2	170		S*	158			
	S	125	5.8	5.1	3	Ce		71	9.3	1.0	156	
	1136+420	T	292	52.2	31.1	103		N1	95	8.8	4.3	3
1159+395		N1	198	5.2	3.3	179		N2	213	15.1	6.1	123
		N2	130	21.3	9.4	167						
		S1	165	6.7	4.8	141						

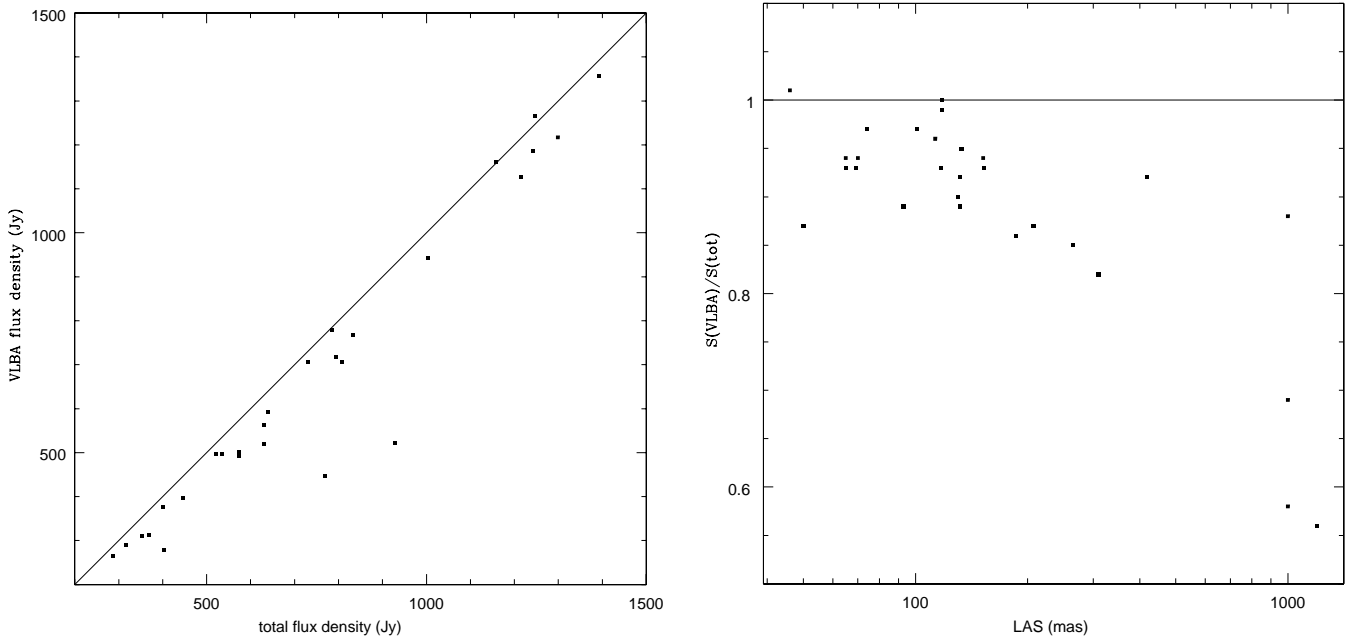


Fig. 2. (*left*): comparison between the VLBA integrated flux densities and total flux densities interpolated from the literature. The line has a slope of one. (*right*): ratio between the VLBA and the total flux density is shown as a function of the overall source angular size.

are larger flux density losses, clearly due to the absence of short uv -spacings (see, as an example, Fig. 4). The two sources with the largest deviations in Fig. 2 (0800+472 and 0809+404) do possess indeed another component detected by the VLA but completely resolved out by the VLBA baselines (see also next section).

4. Comments on individual sources

– 0800+472: the source has an overall extent of ~ 1 arcsec in the VLA 8.4 GHz image (see Paper I). About 40% of the flux density is missing in our VLBA image. Since $\sim 90\%$ of the 8.4 GHz flux density originates within a region of ~ 120 mas, it is likely that most of the missing flux density is on angular scales of this order. The VLBA source structure is strongly bent and the bending probably continues to match the arcsec structure. It is possible that we are in presence of an asymmetric core-jet, with a weak core, as in Stanghellini et al. (2001).

– 0809+404: at arcsec scale the source appears as a very asymmetric double, with $1.2''$ separation and a flux density ratio $\sim 100:1$ at 4.9 GHz (see Paper I). The structure we see here corresponds to the brighter component and is rather amorphous, with the PA of the major axis misaligned by $\sim 40^\circ$ with respect to the orientation of the outer weak component. About 45% of the total flux density is missing in our VLBA observations.

– 1007+422: about 15% of total flux density is missing in our VLBA observations.

– 1044+454: on the arcsec scale the source appears as a very asymmetric double, with flux density ratio $\sim 20:1$ at 4.9 GHz (see Paper I). On the VLBA scale the structure

of the northernmost brighter component is again double and asymmetric, along the same PA but on a \sim six times smaller scale. The source could be either a core-jet with a weak core or a very asymmetric MSO. About 12% of the total flux density is missing in our VLBA observations.

– 1049+384: About 12% of the total flux density is missing in our VLBA observations.

– 1136+420: on the arcsec scale the source appears as a very asymmetric double, with flux density ratio $\sim 20:1$ at 4.9 GHz (see Paper I), roughly oriented in the East–West direction. At VLBA resolution only the brighter component is visible and displays a very amorphous structure. About 30% of the total flux density is missing in our VLBA observations.

– 1314+453: about 15% of the total flux density is missing in the VLBA image.

– 1343+386: a weak feature, accounting for ~ 9 mJy is present to the North of the major components.

– 1432+428: a weak feature, accounting for ~ 10 mJy is present to the South of the major components. About 13% of the total flux density is missing in our VLBA observations.

– 2348+450: about 20% of total flux density is missing in the VLBA image.

5. Discussion

The VLBA observations have produced images with sufficient resolution to describe the source morphology for the large majority of cases.

The present observations do not allow to pick up the radio core, due to the relatively low observing frequency,

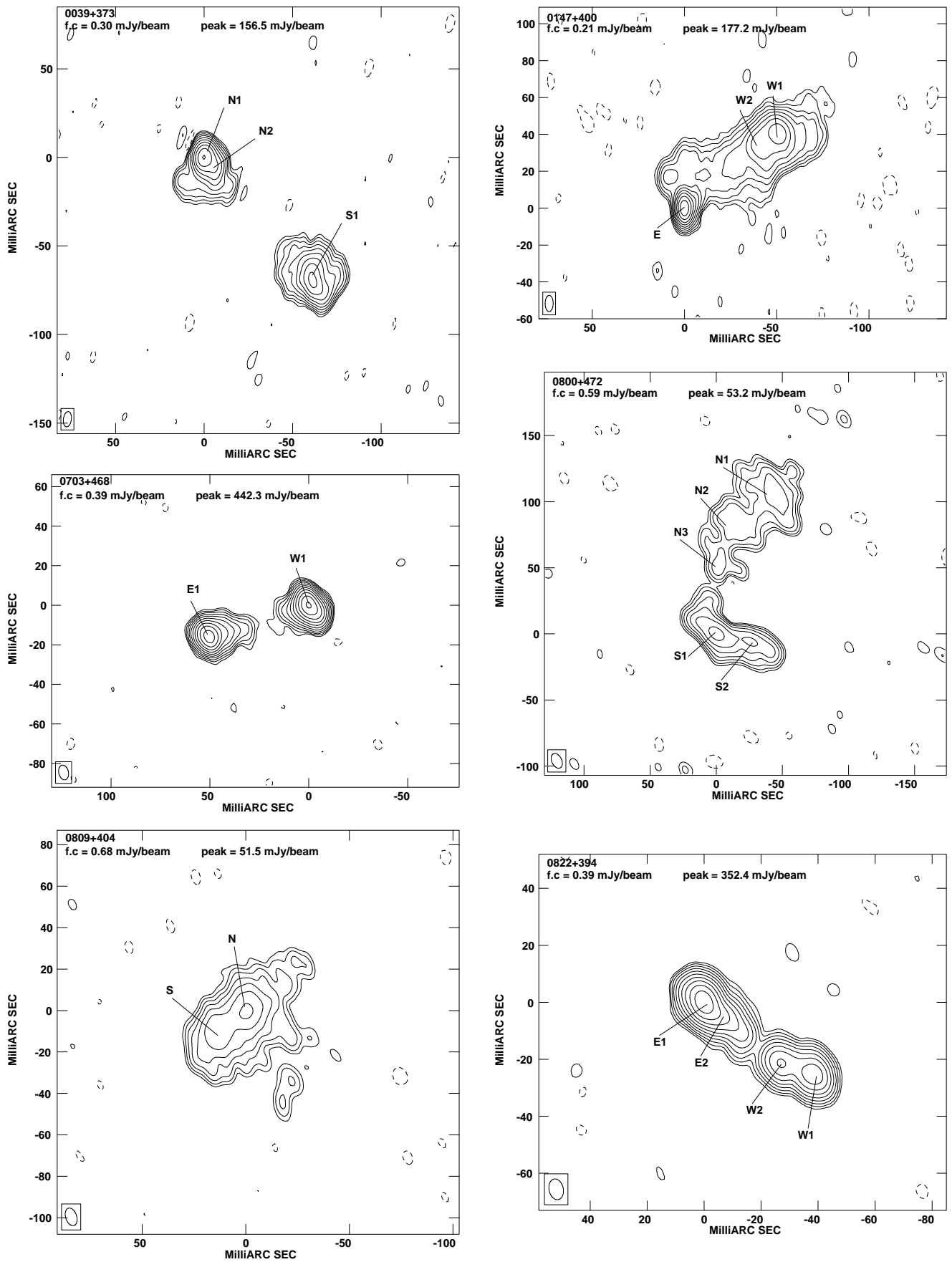


Fig. 3. VLBA images: the first contour (f.c) is generally three times the rms noise level on the image; contour levels increase by a factor of 2; the restoring beam is shown in the bottom left corner in each image.

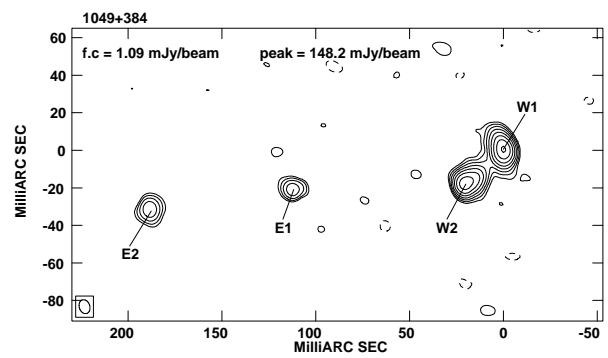
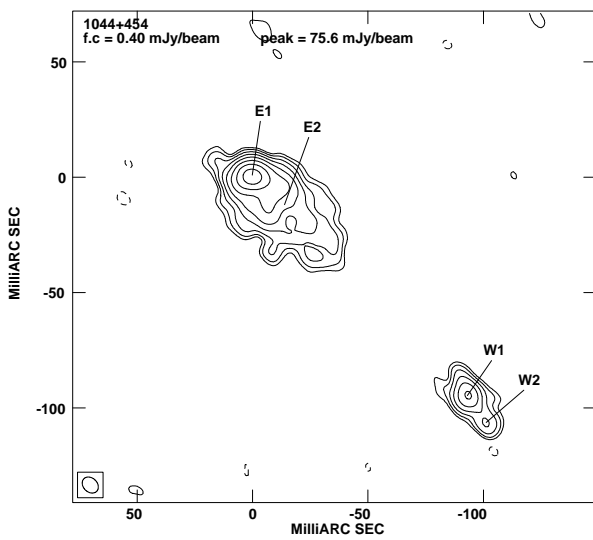
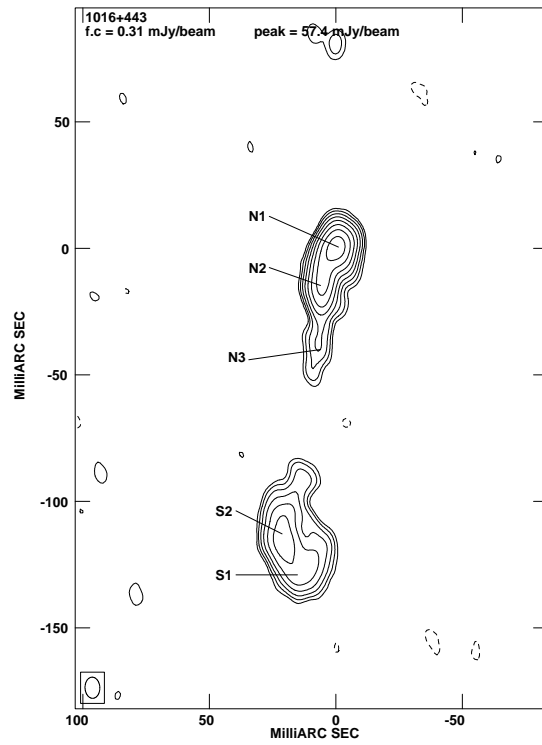
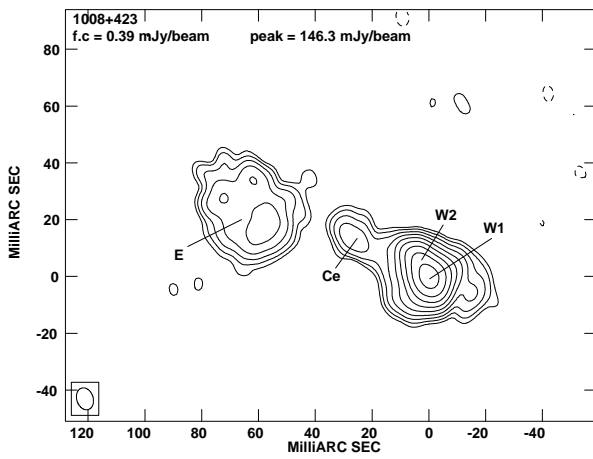
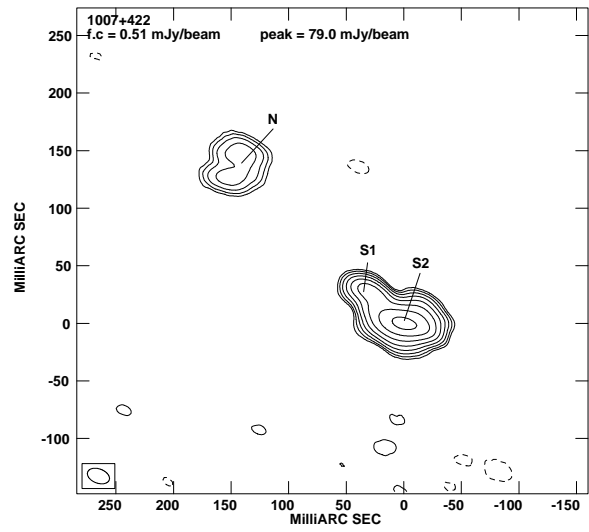
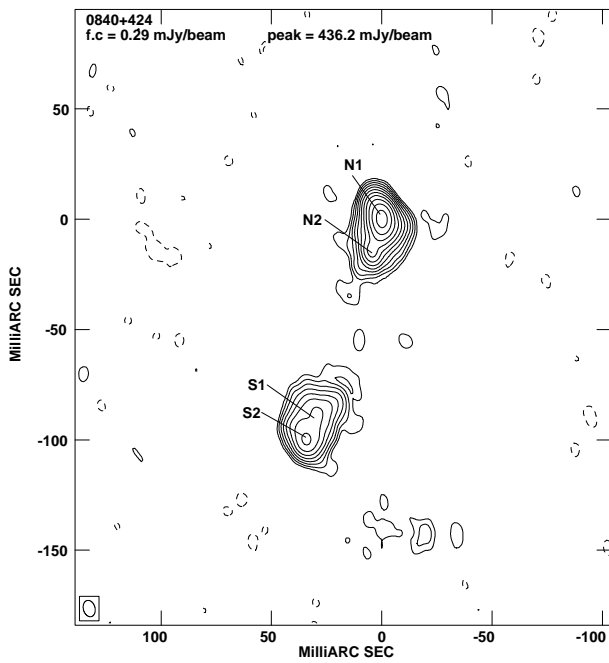


Fig. 3. continued.

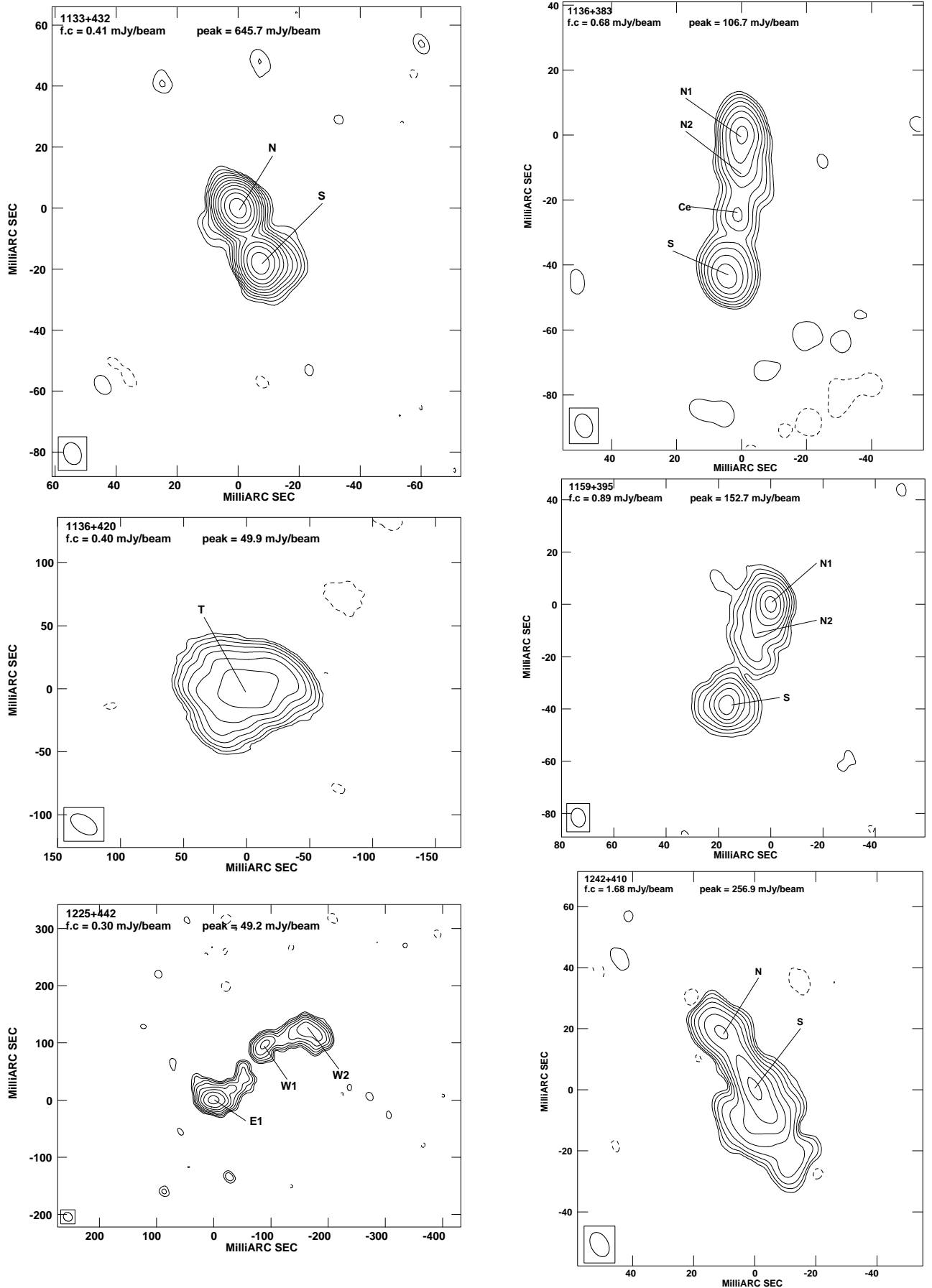


Fig. 3. continued.

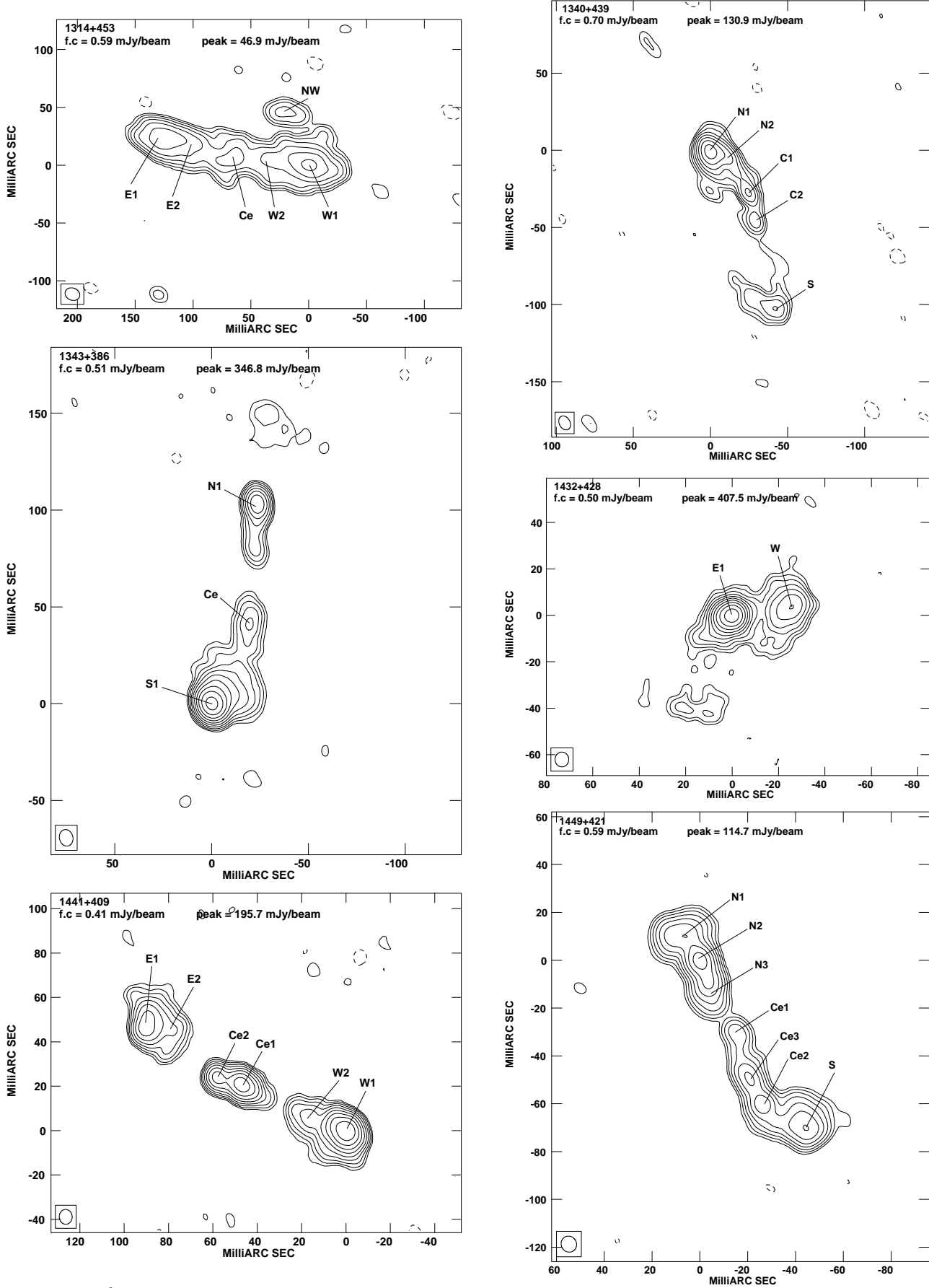


Fig. 3. continued.

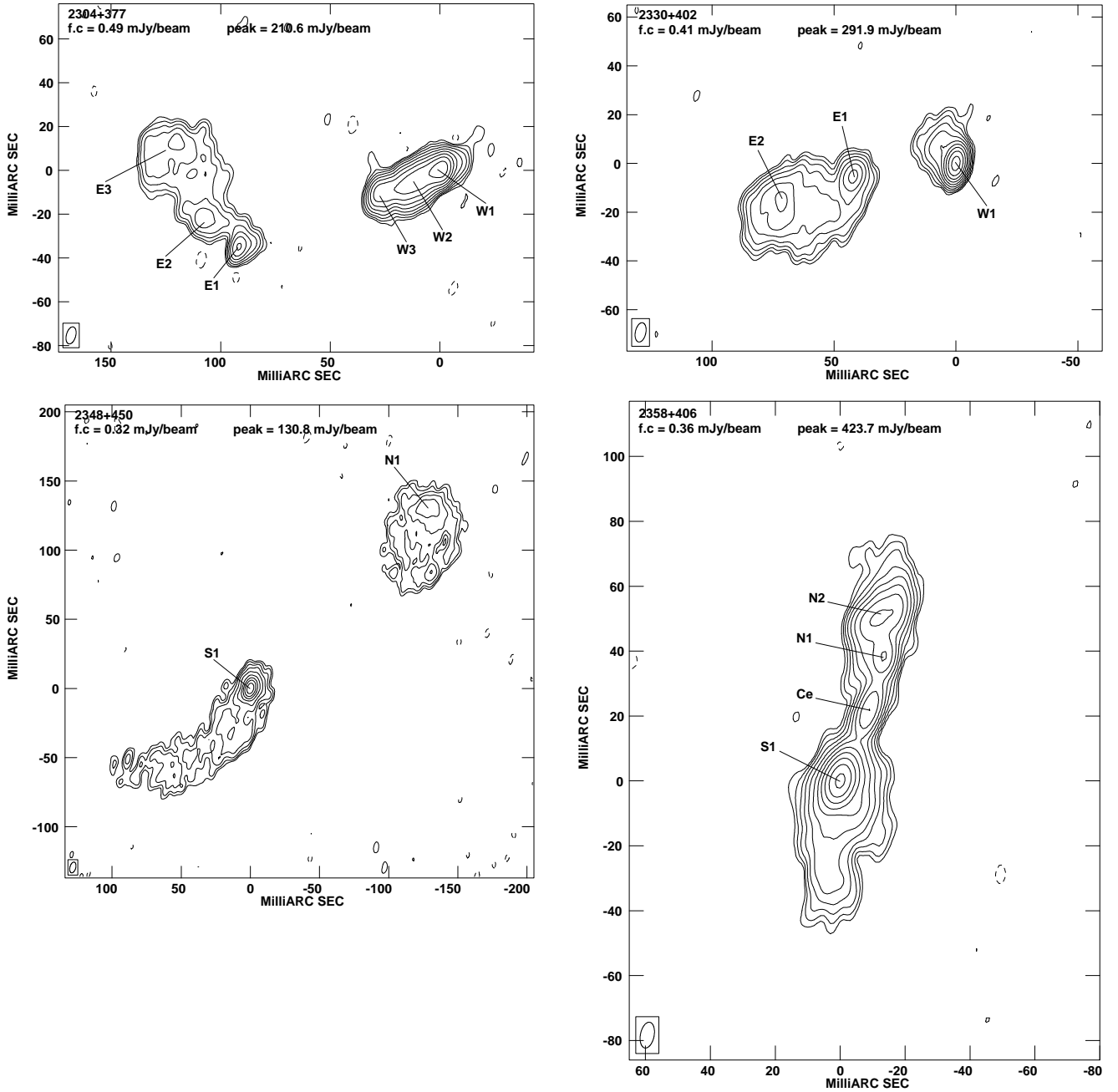


Fig. 3. continued.

but the overall morphology strongly indicates that the sources are mostly two-sided. We see either well separated lobes or lobes connected by bridges, possibly jets. Most sources are edge brightened, suggesting the presence of hot spots, in general not fully resolved from the mini-lobe emission, which contribute most of the source flux density. We tentatively classify these sources as CSOs (two of them are actually MSOs). There are also a few objects with edge darkening, as B3 2304+377, B3 2348+450 and B3 2358+406. There are a number of sources where a compact component, centrally located, could be the source core. However, having only one relatively low frequency we are not in the position to make a definitive statement about core identifications.

Some asymmetries in the flux densities of the two sides are seen, as also some moderate distortions. B3 0800+472 and B3 2304+377 are extreme examples. The sources B3 1225+442 and B3 1449+421 are reminiscent of an *S* morphology (see also Stanghellini et al. 2001).

The average ratio between the component size transverse to the source axis (θ_{trans}) and Largest Angular Size (*LAS*) is $\theta_{\text{trans}}/\text{LAS} \sim 0.08 \pm 0.02$, consistent with findings in other source samples (e.g. Fanti et al. 1990).

We have computed the equipartition parameters for the source components, under the following assumptions: a) proton to electron energy ratio of one; b) filling factor of one; c) maximum and minimum electron (and proton) energies corresponding to synchrotron emission in the

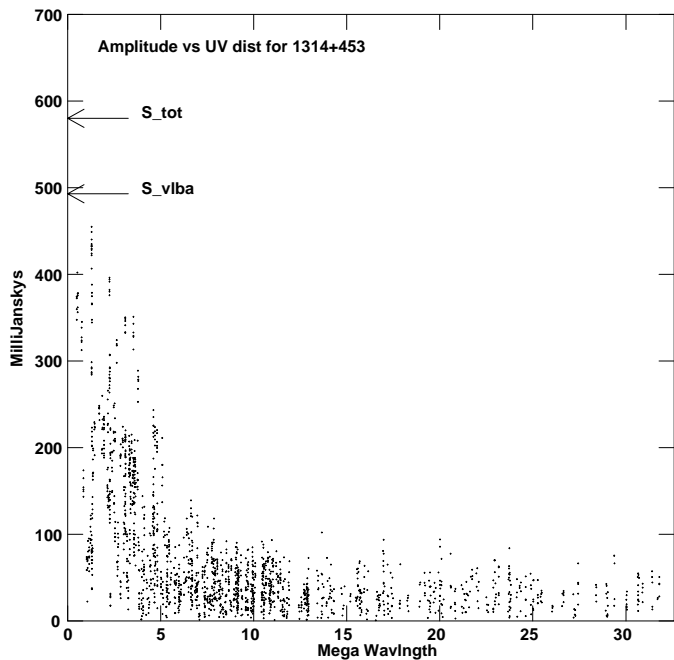


Fig. 4. Plot of the correlated flux density versus projected baseline for the source B3 1314+453. The horizontal arrows indicate the integrated flux density in the VLBA image and total flux density from the VLA as given in Table 1.

frequency range 100 GHz to 10 MHz; d) ellipsoidal volumes with axis corresponding to the observed ones. We also computed the brightness temperatures (T_B) of each component. In order to make easier the reading of the paper, we do not report the individual component values, since they can be obtained from the parameters in Table 2, but only mention the typical values.

The magnetic fields are in the range of several mGauss, going up to ~ 20 mGauss in the most compact components (e.g. B3 1133+432). Brightness temperatures range from $\sim 10^8$ up to $\leq 10^{11}$ K.

6. Conclusions and future plans

We have presented the results of VLBA observations of the most compact sources ($LAS \lesssim 1''$) in the B3-VLBA CSS sample from Paper I.

The large majority of sources have a “double type” structure, with sizes ranging from $\sim 200 h^{-1}$ pc to $\sim 1 h^{-1}$ kpc. Together with the VLA data on the large size sources and with EVN & MERLIN data, presented in Dallacasa et al. (2002, Paper III) on intermediate size

sources, we have at the end a new determination of the Linear Size distribution in the range $\sim 0.2 h^{-1} < LS$ (kpc) $< 20 h^{-1}$. This is an important piece of information to test the source evolution model. We will discuss it in a separate paper.

The sources presented here have just been observed with the VLBA at higher frequencies, with the aim of detecting the radio core, therefore obtaining an unambiguous classification, and of studying the structure of the hot spots. The results will be presented in a forthcoming paper.

Acknowledgements. This work has been partially supported by the Italian MURST under grant COFIN-2001-02-8773. The VLBA is operated by the U.S. National Radio Astronomy Observatory which is a facility of the National Science Foundation operated under a cooperative agreement by Associated Universities, Inc.

References

- Baldwin, J. 1982, in Extragalactic radio sources, ed. D. S. Heeschen, & C. M. Wade (Reidel), IAU Symp., 97, 21
- Begelman, M. C. 1996, in CygA: Study of a radio Galaxy, ed. C. Carilli, & D. Harris (Cambridge University Press), 209
- Condon, J. J., Cotton, W. D., Greisen, E. W., et al. 1998, AJ, 115, 1693
- Dallacasa, D., Fanti, C., Giacintucci, S., et al. 2002, A&A, 389, 126 (Paper III)
- Fanti, R., Fanti, C., Schilizzi, R. T., et al. 1990, A&A, 231, 333
- Fanti, C., Fanti, R., Dallacasa, D., et al. 1995, A&A, 302, 317
- Fanti, C. 2000, Proc. of 5th EVN Symp., ed. J. E. Conway, A. G. Polatidis, & R. S. Booth & Y. M. Pihlström, Onsala Space Observatory
- Fanti, C., Pozzi, F., Dallacasa, D., et al. 2001, A&A, 369, 380 (Paper I)
- Fanti, C., & Fanti, R. 2001, Proc. of Issues in Unification of AGNs, ed. R. Maiolino, A. Marconi, & N. Nagar, Osservatorio Astrofisico di Arcetri
- Kaiser, C. R., & Alexander, P. 1997, MNRAS, 286, 215
- Murgia, M., Fanti, C., Fanti, R., et al. 1999, A&A, 345, 769
- O’Dea, C. P., & Baum, S. A. 1997, AJ, 113, 148
- O’Dea, C. P. 1998, PASP, 110, 493
- Polatidis, A., Wilkinson, P. N., Xu, W., et al. 1999, New Astr. Rev., 43, 657
- Readhead, A. C. S., Taylor, G. B., Xu, W., et al. 1996, ApJ, 460, 634
- Stanghellini, C., Dallacasa, D., O’Dea, C. P., et al. 2001, A&A, 377, 377
- Vigotti, M., Grueff, G., Perley, R., et al. 1989, AJ, 98, 419